

A study of photoexcited carrier relaxation in $\text{YBa}_2\text{Cu}_3\text{O}_{7-\delta}$ by picosecond resonant Raman spectroscopy

T. Mertelj

*Jozef Stefan Institute, Jamova 39, 1000 Ljubljana, Slovenia and
Faculty of Mathematics and Physics, Jadranska 19, 1000 Ljubljana, Slovenia*

J. Demsar, B. Podobnik, I. Poberaj, D. Mihailovic
Jozef Stefan Institute, Jamova 39, 1000 Ljubljana, Slovenia
(March 12, 2018)

The temperature dependence of the energy relaxation of photoexcited (PE) carriers is used as a probe of the electronic structure of $\text{YBa}_2\text{Cu}_3\text{O}_{7-\delta}$ in the insulating ($\delta \approx 0.8$) and metallic ($\delta \approx 0.1$) phases. The energy relaxation rate to phonons is obtained by measuring the non-equilibrium phonon occupation number, n_{neq} , with pulsed Raman Stokes/anti-Stokes spectroscopy using 1.5 and 70 ps long laser pulses. We can distinguish between relaxation via extended band states and localized states, since theoretically in the former, the relaxation is expected to be virtually T -independent, while in the latter it is strongly T -dependent. From the experiment - which shows strong temperature dependence of n_{neq} - we deduce that at least part of the PE carrier relaxation proceeds via hopping between localized states and we propose a simple theoretical model of the relaxation process. In addition, we compare the coupling of different vibrational modes to the carriers to find that the apical O vibrational mode is significantly more involved in the energy relaxation process than the in-plane 340 cm^{-1} mode. This implies that the localized states are mainly (but not entirely) coupled to out-of plane vibrations.

I. INTRODUCTION

An important question in high- T_c cuprates is whether the carriers that lead to superconductivity in these materials can be described to be in localized polaronic (magnetic or phononic) states or are in extended, band-like states, albeit somewhat deviating from usual Fermi Liquid behavior due to the shape of the Fermi surface. Since both views can be supported by experimental observations¹, either dual interpretations are possible, whereby the experimental data can be explained in either picture, or actually both types of carriers are present simultaneously. The latter immediately leads to the possibility of a two component superconductivity scenario, for example a Boson-Fermion scenario² or a 2+1 dimensional superconductivity scenario³ or even excitonic superconductivity⁴. Experimentally, the presence of localized states in the metallic phase of the cuprates is suggested (amongst others) by photoconductivity measurements on the insulating precursor $\text{YBa}_2\text{Cu}_3\text{O}_{7-\delta}$ ($0.6 < \delta < 1.0$)⁵, which show unambiguously that i) there are states within 2 eV of E_F which are localized and ii) that at the insulator-to-metal transition only the carriers near E_F change their character giving rise to a cross-over from semiconducting to insulating low-frequency conductivity $\sigma(\omega \rightarrow 0)$, while $\sigma(\omega)$ for $> 800 \text{ cm}^{-1}$ (0.1 eV) changes only gradually with doping and thus it is quite likely that states further away from E_F remain localized and Fermi glass-like in the metallic phase.

In general, it is not possible to ascertain whether electronic states are localized or extended using spectroscopy methods which measure the single particle or joint density of states. More indirect methods are required, especially for $|E - E_F| > kT$. By investigating the process of carrier relaxation and energy loss from photoexcited states using Raman spectroscopy, we present evidence of temperature-activated PE carrier relaxation through localized states within $\sim 2 \text{ eV}$ of E_F in insulating *and metallic* $\text{YBa}_2\text{Cu}_3\text{O}_{7-\delta}$ (with $\delta \approx 0.8$ and $\delta \approx 0.1$ respectively).

To enable quantitative measurements of the phonon occupation numbers and avoid possible misinterpretation of these results, we have employed extensive calibration and correction procedures to quantitatively measure the Raman Stokes and anti-Stokes intensities enabling an accurate interpretation of the carrier relaxation process. These are described in detail in the first Section of the paper. In the second Section, we present the experimental results for different YBCO samples with a discussion of calibration procedures and possible artifacts, and in the Discussion we first discuss the connection between the carrier relaxation and the observable quantities, then we suggest a model to explain the relaxation process and finally discuss the origin of the localized states in the context of the established knowledge about the electronic structure of the material. The conclusions regarding the existence of localized states are reached without assumptions about the mechanism for the electron-phonon interaction and the PE process.

II. EXPERIMENTAL TECHNIQUE AND INTENSITY CALIBRATION PROCEDURE

The experimental technique used to measure the phonon shake-off entails the measurement of the non-equilibrium phonon occupation number n_{neq} by measurement of the Stokes (S) and anti-Stokes (A) Raman scattering intensities on a picosecond timescale. Details of the pulsed Raman scattering experimental setup have been given previously⁶. The experiment is performed by exciting carriers and simultaneously measuring Raman scattered light with 1.5 ps or 70 ps laser pulses. These are generated by frequency doubling a pulse-compressed (1.5 ps) or non-compressed (100 ps) mode-locked Nd:YAG laser. The resulting photon energy 2.33 eV (532 nm) is sufficient to excite inter-band transitions in the material both within the CuO₂ planes and between the CuO₂ planes and the Cu-O chains depending on the polarization of the incident light.⁷ The photon flux used is typically 10¹³ photons/cm²/pulse, with estimated peak PE-carrier densities $n_c \approx 10^{18}$ cm⁻³.

The measurements of n_{neq} were performed on YBCO single crystals with $\delta \approx 0.1$ (twinned) and $\delta \approx 0.8$ mounted in a liquid-He flow cryostat. The data are analyzed for the A_g oxygen 340-cm⁻¹ plane-buckling vibration (B_{1g} in tetragonal symmetry) and the $A_g(A_{1g})$ 500-cm⁻¹ apical O(4) Raman-active vibrations. The integrated intensities of the S and A phonon lines are obtained by fitting to either a Gaussian or Lorentzian lineshape in the temperature range 100 - 320 K. The Gaussian lineshape was mainly used for the 340 cm⁻¹ mode, where the frequency resolution of the spectrometer limited the linewidth.

The ratio of the Stokes and anti-Stokes Raman intensities in backscattering geometry is given by:

$$\frac{I_S(t)}{I_A(t)} = \frac{\xi(\omega_L, \omega_S) \omega_S \eta(\omega_S) \Theta_{ab}(\omega_L, \omega_S, \omega_p) n_p(t) + 1}{\xi(\omega_L, \omega_A) \omega_A \eta(\omega_A) \Theta_{ba}(\omega_A, \omega_L, \omega_p) n_p(t)}. \quad (1)$$

Here ω_p is the phonon frequency, n_p is the phonon occupation number, $\hbar\omega_L$ is the incident-photon energy, $\hbar\omega_S$ and $\hbar\omega_A$ the S and A scattered-photon energies respectively, $\eta(\omega)$ is the frequency dependent refractive index of the crystal and Θ_{ab} is the appropriate Stokes component of the Raman tensor for incident polarization a and scattered polarization b while Θ_{ba} is the same for anti-Stokes scattering. We take into account that due to time-reversal symmetry $\Theta_{ab}(\omega_L, \omega_A, -\omega_p) = \Theta_{ba}(\omega_A, \omega_L, \omega_p)$ ⁸. The factor $\xi(\omega_L, \omega)$ takes into account penetration depth and reflection of incident and scattered light on the surface of the crystal at ω_L and ω_S or ω_A , as well as diffraction of the scattered light upon exiting the crystal⁹:

$$\xi(\omega_L, \omega) = \frac{(1 - \Re(\omega_L))(1 - \Re(\omega))}{\kappa(\omega_L) + \kappa(\omega)} \frac{1}{\eta^2(\omega)}, \quad (2)$$

where $\Re(\omega)$ and $\kappa(\omega)$ are the reflectivity and the absorption coefficients respectively.

Since it is known from experiment that the photoinduced reflectivity change $\Delta\Re/\Re \sim 10^{-3}$ for photoexcited carrier densities¹⁰ of $\sim 10^{21}$ cm⁻³, we assume that the change in optical constants by photoexcited carriers with our carrier densities typically of $\sim 10^{18}$ cm⁻³ is sufficiently small to ignore. Since the relevant matrix elements for both the Raman and dielectric tensors are related to each other, we assume that the same also holds for the Raman tensor $\Theta(\omega_L, \omega_S, \omega_p)$.

The non-equilibrium phonon occupation number is defined by $n_{neq}(t) = n_p(t) - n_{eq}(\omega_p, T)$, where at temperature T for a phonon with frequency ω_p , n_{eq} is given by:

$$n_{eq}(\omega_p, T) = \left[\exp\left(\frac{\hbar\omega_p}{k_B T}\right) - 1 \right]^{-1}. \quad (3)$$

Since we are performing photoexcitation and Raman scattering with the same laser pulse, the measured non-equilibrium phonon occupation number is a weighted time average over the probe laser pulse duration:

$$n_{neq} = \frac{\int g(t) n_{neq}(t) dt}{\int g(t) dt} \quad (4)$$

where $g(t)$ represents temporal shape of the laser pulse.

To obtain accurate values of n_{neq} one must take into account for the fact that magnitudes of the Raman tensor components and the optical constants are different for S and A photons due to the finite width of the resonances with electronic states. Fortunately resonance Raman scattering (RRS) has been extensively investigated in YBa₂Cu₃O_{7- δ} ^{11,12} and we use these data together with dielectric constant data⁷ to calculate n_{neq} from the measured S and A intensities.

The spectrometer spectral response was calibrated by measuring the spectrum of a tungsten lamp mounted in place of the sample. We assume that the lamp spectrum is proportional to a black-body spectrum in the frequency range

of interest.¹³ Since there was a spread in the ratio of the spectral responses at ω_S and ω_A due to spectrometer grating filling effects and lamp alignment, we averaged over several calibration cycles to determine the spectrometer response. To check our calibration procedure and whether the frequency dependence of the Raman tensor and optical constants taken from the literature give the correct value of n_p , the CW-laser intensity dependence of the phonon temperature T_p was determined from the I_S/I_A ratio. The phonon temperature is then given by

$$T_p = \frac{\hbar\omega_p}{k_B \ln\left(\gamma_p \frac{I_S}{I_A}\right)} \quad (5)$$

where γ_p is the calibration constant to be determined for the phonon p including correction factors for the frequency dependence of the spectrometer spectral response as well as the frequency dependence of the Raman tensor and optical constants. To check whether γ_p is correctly determined, we measure T_p (as determined using Eq. 5) using a CW laser as a function of laser power where under stationary conditions, the phonon temperature is equal to the lattice temperature in the scattering volume. We find that T_p extrapolates to the ambient temperature at zero incident laser power, confirming that our calibration procedure is correct and giving an error in T_p of less than a 10 K.

The lattice temperature T_0 of the scattering-volume is somewhat higher than the ambient cryostat temperature due to absorption of laser energy. This needs to be corrected for if we wish to obtain an accurate value for $n_p(T)$ from our measurements. The temperature rise in the scattering-volume can be divided into two parts. The first part, ΔT_{CW} is a time-independent average rise of temperature which is a consequence of heat buildup in the sample. This is very similar to the heating due to absorption of a CW-laser beam with equivalent beam parameters and average power, and depends on the sample geometry, the sample thermal conductivities and thermal coupling of the sample to the sample holder. Since all three components of the thermal conductivity tensor in YBCO are virtually temperature independent down to 100K¹⁴, this is also true for ΔT_{CW} . We thus use the room-temperature value of ΔT_{CW} measured with an Ar⁺-ion CW laser with a photon energy of 2.41 eV (c.f. 2.33 eV for the Nd:YAG) as a function of laser power P_0 to obtain an accurate calibration of ΔT_{CW} versus P_0 .

The second correction is the transient temperature rise due to each pulse ΔT_{tr} , and is determined mainly by the heat capacity of the scattering volume. We calculate^{15,16} that there is only a $\sim 50\%$ increase in the transient part of ΔT for the 1.5 ps pulses in comparison to the 70 ps pulses, from which we deduce that most of the generated heat remains in the scattering volume for the duration of the laser pulse. ΔT_{tr} is calculated¹⁶ to be below 0.5 K/mW for both 1.5 ps and 70 ps pulse lengths when focused to a 30 μm diameter spot. This is an order of magnitude smaller than the observed phonon heating determined from the ratio of the S and A phonon intensities at room temperature and is therefore neglected. Below 120 K, the non-equilibrium effects we are trying to measure become comparable to the effects of the time dependent part of the temperature increase ΔT_{tr} , and so we do not discuss data below this temperature.

III. EXPERIMENTAL RESULTS

A. The nonequilibrium phonon temperature and nonequilibrium occupation numbers

The normalized Raman spectra at different temperatures for YBCO with $\delta \approx 0.1$ are shown in Fig. 1 for the two different polarizations showing the A and S spectra of the two phonons. We see that the A peaks become smaller with decreasing temperature and disappear below 100 K. The temperature dependence of the nonequilibrium phonon temperature ΔT_p , defined as $\Delta T_p = T_p - T_0$ is plotted in Figs. 2 and 3 for $\delta \approx 0.8$ and $\delta \approx 0.1$ respectively. In both cases panel a) shows the apical 500 cm^{-1} phonon and panel b) the 340 cm^{-1} phonon values.

In the $\delta \approx 0.8$ sample (Fig.2), a significant nonequilibrium phonon heating is observed *only* for the 1.5 ps-pulse excitation. The nonequilibrium apical-oxygen phonon heating is the most significant, reaching 250K at room temperature. With decreasing temperature, the heating monotonically drops and it saturates at $\Delta T_p \sim 30\text{K}$ below 100K. On the other hand, the nonequilibrium planar-buckling-phonon heating is smaller and it drops faster with decreasing temperature reaching a minimum around 150 K. Below 100 K, ΔT_p rises again with decreasing temperature because of the drop in the heat capacity below this temperature results in a measurable transient increase in the lattice temperature as discussed in the previous section.

In the $\delta \approx 0.1$ sample, similar nonequilibrium heating is observed for both laser pulse lengths at room temperature(Fig. 3). However, the actual values of ΔT_p are smaller than in the $\delta \approx 0.8$ sample. Temperature dependence of the nonequilibrium apical-oxygen phonon heating is different for the different excitation-pulse lengths (Fig. 3a): with 1.5-ps pulse excitation, ΔT_p steeply drops with decreasing temperature and reaches zero between 200-250K. The drop of ΔT_p with decreasing temperature is less steep with 70-ps laser excitation and saturates at $\sim 25\text{K}$ below 200K.

The planar 340 cm^{-1} phonon in the $\delta \approx 0.1$ sample shows a smaller ΔT_p than the apical-oxygen (Fig. 3b) over the whole range of temperatures, but the difference between phonons is less dramatic than in the $\delta \approx 0.8$ sample. The difference in behavior at different pulse lengths is also less clear for the planar 340 cm^{-1} phonon due to a larger scatter in the data, which is a consequence of the smaller Raman intensity for this phonon at the $\delta \approx 0.1$ doping.

Since the nonequilibrium-phonon occupation number n_{neq} is related to the carrier relaxation rate, its temperature dependence for both phonons is plotted in Arrhenius plots in Fig. 4 for $\delta \approx 0.8$ and Fig. 5 for the $\delta \approx 0.1$. The important observation is that in all cases n_{neq} shows a strong temperature dependence. Fitting the data with an Arrhenius law, we obtain activation energies E_a in the range 56 - 210 meV in the metal ($\delta \approx 0.1$) depending on pulse-length, and 60 - 110 meV in the insulating phase ($\delta \approx 0.8$). Below 120 K the transient laser heating becomes comparable to the effect of n_{neq} , which is probably the reason for the departure from the activated behavior (Fig. 5) at low temperatures. In the metal, for the apical O vibration, measurement with both laser pulse lengths is possible and we observe a significant difference in the activation energy in the two cases, which - as we shall see in the Discussion - arises probably because of the effects of the temperature dependence of the effective carrier lifetime.

B. Discussion of possible artefacts in the Stokes/anti-Stokes ratios

In the measurement of Raman intensities, it is very important to take into account all possible effects, to avoid erroneous interpretation of the results. We thus proceed with a detailed analysis of the possible artefacts with a detailed justification of all the assumptions made. For the calculation of n_{neq} from experimental S/A intensity ratios at different temperatures it was assumed that correction factors and Raman tensor components in (1) are temperature independent. These may nevertheless have some, albeit small temperature dependence, and so the approximation was checked on the basis of data available in the literature. Since only the ratio of the correction factors and Raman tensor components at the Stokes and anti-Stokes frequency appear in expression (1), the frequency dependent part of the change of optical constants and the Raman-tensor component with changing temperature has the largest effect on the calculated n_{neq} , while the frequency independent part of the change has only little effect.

For in-plane polarized light ($E||a, b$) Holcomb *et al.*¹⁸ measured the thermal difference reflectance in a $\delta \approx 0$ YBCO thin film. They find that the quantity

$$\Re(\omega, T)^{-1} \frac{\partial \Re(\omega, T)}{\partial T}, \quad (6)$$

is below $4 \cdot 10^{-4}\text{K}^{-1}$ around 2.3 eV photon energy in the 90-300K temperature range and the difference of its values at ω_S and ω_A is below $\sim 10^{-4}\text{K}^{-1}$. By taking into account that the reflectivity around this energy⁷ is 0.14 the total change of reflectivity in this temperature range is estimated to be ~ 0.012 , giving relative change of $\sim 8\%$ with a difference at ω_S and ω_A of $\sim 2\%$. Because this is too small to be observed in our measurements it is ignored.

Inferring further from the work of Fugol *et al.*¹⁹, the optical absorption in $\delta \approx 0.15$ YBCO film increases linearly by $\sim 2\%$ with increasing temperature in the temperature range 100K-140K. Extrapolating to room temperature this would give a 10% increase at 300K. However, the increase is almost the same at 1.7eV and 2.7 eV indicating a weak frequency dependence and hence this would have negligible effect on the ratio of S and A intensities. The Raman-tensor component for the incident and scattered light polarizations parallel to the CuO_2 planes decreases with increasing temperature by $\sim 25\%$,²⁰ but again the decrease is virtually the same at 2.34eV and 2.6eV and is very similar at 1.92eV having no effect on the S/A ratio or n_{neq} .

The changes of the *frequency dependence* of optical constants and the Raman-tensor component with temperature for light polarized parallel to the CuO_2 planes is therefore estimated to be small enough that the correction factors for the planar buckling-phonon can be considered temperature independent in our experiment.

Regarding the c-axis polarized optical response, as far as we are aware there are no published temperature dependence data for the visible region. However, for $\delta \approx 0.1$ the low temperature resonant Raman scattering data¹¹ give the same value of the S/A intensity correction factor at room temperature as measured by the CW Ar^+ laser measurement, indicating that its temperature dependence is negligibly small.

For $\delta \approx 0.8$, the experimental data on the temperature dependence of optical response in visible region are also not available. The data of Fugol *et al.*¹⁹ indicate that absorption for light polarized parallel to the CuO_2 planes in a $\delta \approx 0.7$ YBCO film is almost temperature independent at 2.7 eV while it shows temperature dependence in the region of the 1.75-eV Cu-O charge-transfer absorption peak. However, since this peak does not extend above 2eV, we expect that it does not influence absorption at 2.33 eV significantly. In the absence of other experimental data we expect that also for $\delta \approx 0.8$ YBCO temperature dependence of the correction constants is small enough that it does not significantly influence our interpretation of the results, while the data for $\delta \approx 0.1$ are in principle more reliable, and the assumptions are experimentally verified. In summary all the necessary correction factors can be accurately obtained and cross-checked experimentally giving us confidence of the accuracy of the measured n_{neq} .

IV. DISCUSSION

A. Estimate of the carrier lifetime and discussion of the probing process

In a system as complex as YBCO there are many low energy excitations apart from optical phonons (e.g. magnons) that can take up the relaxing-PE-carrier energy. In our experiment, only the optical-phonon part of the relaxed energy can be accessed. Despite unknown branching ratios to observed optical phonons, the magnitude of the effective PE-carrier lifetime can be estimated by comparing data for the 1.5 ps and 70 ps experiments in terms of a simple model.

In the model we describe the PE carriers with their volume density, n_c , and the effective lifetime τ_c . The effective lifetime includes the PE-carrier relaxation to all possible channels. The time-dependence of the carrier number density n_c is given by a simple relaxation-time approximation:

$$\frac{dn_c(t)}{dt} = -\frac{n_c(t)}{\tau_c} + \kappa g(t), \quad (7)$$

where κ is the absorption coefficient and $g(t)$ is the incident photon flux density following the temporal profile of the laser pulse. Assuming that at least a part of the PE-carrier energy is transferred to optical phonons whose anharmonic lifetime is τ_p (A part of the PE carrier energy may be as well transferred to other low energy excitations.), the time dependence of n_{neq} is described by:

$$\frac{dn_{neq}(t)}{dt} = -\frac{n_{neq}(t)}{\tau_p} + \frac{c_{pc}}{N_p} \frac{n_c(t)}{\tau_c}. \quad (8)$$

The second term on the right hand side is the phonon generation rate where c_{pc} is the average number of phonons created by a carrier, which implicitly includes also the branching ratio to optical phonons, and N_p is the number of different phonon modes per volume unit involved in the relaxation process.

Since a pump pulse is simultaneously a probe, the measured nonequilibrium-phonon occupation number n_{neq} is given by the equation (4). The laser pulse shape $g(t)$ is assumed to have a Gaussian temporal profile,

$$g(t) = \sqrt{\frac{2}{\pi}} j_0 \frac{T}{\tau_L} \exp\left(-\frac{2t^2}{\tau_L^2}\right) \quad (9)$$

where τ_L is the laser pulse length, T the pulse repetition period and j_0 the average photon flux density.

Equations (7), (8) and (4) are numerically integrated to obtain n_{neq} as a function of the inverse PE-carrier relaxation time, τ_c^{-1} . The resulting curves for the two experimental pulse lengths and different phonon lifetimes are shown in Fig. 6. For 1.5-ps pulses n_{neq} increases almost linearly with increasing τ_c^{-1} for long PE-carrier lifetimes and it saturates when τ_c^{-1} approaches τ_L^{-1} . For the 70-ps pulses the initial increase is less steep, saturation is stronger due to smaller value of τ_L^{-1} and it sets in at smaller values of τ_c^{-1} . For both pulse lengths n_{neq} increases with increasing phonon lifetime with a stronger increase for the 70-ps pulses.

To enable comparison of the experimental data with the model, we estimate the phonon lifetimes from the phonon Raman linewidths. At room temperature for $\delta \approx 0.1$, $\Delta\omega \approx 50 \text{ cm}^{-1}$ and $\Delta\omega \approx 20 \text{ cm}^{-1}$ for the apical-oxygen phonon and the planar buckling phonon respectively. For $\delta \approx 0.8$, the apical-oxygen phonon linewidth is $\Delta\omega \approx 30 \text{ cm}^{-1}$ and the planar-buckling phonon one is $\Delta\omega \approx 18 \text{ cm}^{-1}$. Although this includes also inhomogeneous broadening we can estimate the lower limit for the phonon lifetimes which is sufficient for our discussion. We obtain $\tau_p \sim 0.2 \text{ ps}$ for the apical-oxygen phonon and $\tau_p \sim 0.4 \text{ ps}$ for the planar buckling phonon. This is consistent with the values of $\sim 0.5 \text{ ps}$ obtained for both phonons from experimental temperature dependencies of phonon linewidths^{21–23}.

The room temperature value of n_{neq} in the superconducting sample with $\delta \approx 0.1$ is nearly the same for both 1.5 and 70 ps pulse lengths. Taking the room temperature phonon lifetime of $\sim 0.5 \text{ ps}$ we estimate from the crossection of the curves for $\tau_p = 0.5 \text{ ps}$ (the curves with square symbols) in Fig. 6 an effective PE-carrier-energy lifetime to be in the range $10 \sim 100 \text{ ps}$. Here we use the fact, that the position of the crossection along abscise does not depend on the unknown coupling parameter $\frac{c_{pc}}{N_p}$ and therefore on the branching ratios to different excitations. We stress here that this is an estimate of the time it takes for the carrier to reach equilibrium and not of its lifetime in the excited state as implied by the model, which uses only a simple relaxation-time approximation for description of the PE-carrier system.

Using the result that the phonon lifetime is apparently much smaller then the effective PE-carrier lifetime, the number of emitted phonons per unit volume is:

$$N_p \approx \frac{c_{pc}}{n_{neq}} \frac{\tau_p}{\tau_c} n_c. \quad (10)$$

In our experiment, the PE-carrier density $n_c \sim 4 \times 10^{18} \text{ cm}^{-3}$. Since the photon energy is 2.33 eV and the phonon energy of $\sim 50 \text{ meV}$, $10 \sim 40$ phonons are released per absorbed photon. Taking the room temperature experimental value of n_{neq} , we get $N_p \sim 10^{18} \text{ cm}^{-3}$ which is much smaller than the density of phonon modes in an optical-phonon branch. Since Raman scattering probes the phonons with wavevectors near the center of the Brillouin zone, this would imply that the PE carriers relax primarily by emitting low momentum optical phonons near the center of the Brillouin zone. Alternatively, in a scenario which is consistent with the relaxation mechanism proposed in the next section - together with the low dispersion and short anharmonic lifetime of the optical phonons - the k -selection rule is no longer valid and the vibrational modes excited by carriers are local modes for which the Raman $k \rightarrow 0$ selection rule is not relevant.

From Fig. 6 it can be seen that n_{neq} increases with increasing phonon lifetime and decreases with decreasing PE-carrier relaxation rate τ_c^{-1} . Since τ_p increases slightly with decreasing temperature, we can state with confidence that the observed strong temperature dependence of n_{neq} is not a result of the temperature dependence of τ_p . The temperature dependence of n_{neq} can as well be a consequence of temperature dependence of the coupling parameter $\frac{c_{pc}}{N_p}$. In this case however, the observed temperature dependence of n_{neq} should be the same for different excitation laser pulse lengths, which is not the case in our experiment. We therefore conclude that the observed strong temperature dependence of n_{neq} is mostly a consequence of a decrease of the PE-carrier energy relaxation rate with decreasing temperature.

B. Carrier relaxation via localized states

The hot-carrier energy relaxation rate, r_E , in semiconductors with hot-carrier energy $E \gg kT$ and where carriers are assumed to relax via *extended* states, is virtually independent of the lattice temperature irrespective of whether the electron-phonon interaction is via deformation potential or via polar optical scattering.²⁴

In contrast, the measurements of n_{neq} in YBCO show a strong temperature dependence of r_E for both $\delta \approx 0.1$ and 0.8. In addition, we find an unusually long room-temperature effective PE-carrier lifetime (which is the total time the carrier is out of equilibrium) so we propose that the PE-carrier relaxation in YBCO proceeds by *hopping through a band of localized states*. There are however other possible mechanisms giving temperature dependence of the PE carrier relaxation rate (e.g. strong band dispersion or/and correlation effects). But the fact, that PE-carrier relaxation virtually freezes out at low temperatures (as indicated by almost two orders of magnitude drop of the n_{neq} with decreasing temperature) definitely favors the PE carrier localization.

The temperature dependence of electronic relaxation in localized state systems has so far been discussed in detail only in the context of charge transport and the frequency-dependent conductivity $\sigma(\omega)$ ²⁵⁻²⁷. The relaxation processes discussed in these works generally consider the hopping behavior of carriers near E_F , since they are interested primarily in low-frequency properties of such materials. In our case the carriers are excited far above equilibrium and so these models can not be directly applied, although the basic mechanisms for hopping can be similar and indeed the predicted temperature dependence of the conductivity is similar as we observe for the PE-carrier energy relaxation rate.

The relaxation of PE carriers can proceed either via intra-gap defect states as in a Fermi glass⁵, or through self-trapped polaron states. The existence of polaronic self-trapped states in superconductor insulator precursors with binding energies in the range of 60 - 100 mV has been known from photoinduced absorption and fits to the mid-infrared region (0.1-0.5 eV)²⁸. The T -dependence of the hopping rate in this case is essentially determined by the barrier height, W which is related to the polaron binding energy E_B and so the temperature dependence of r_E is essentially given by the expression for activated hopping²⁵.

Alternatively in the Fermi-glass picture, the carriers relax to lower energy mainly by tunneling through a cascade of neighboring states. However, occasionally they have to hop upwards because there are no neighboring sites with lower energies available giving rise to a temperature dependent relaxation. The probability for transition upwards is proportional to $w_0 \exp(-W/k_B T)$, where W is the energy difference between neighboring localized states, and w_0 the probability for transition downwards. If p is the probability that during relaxation a carrier hops to a site with all neighboring sites at higher energy then the carrier energy change after N hops is

$$\Delta E = W N p - W N (1 - p) = W N (2p - 1). \quad (11)$$

The average time needed for N hops is

$$\Delta t = N p \left[w_0 \exp\left(-\frac{W}{k_B T}\right) \right]^{-1} + N(1 - p)w_0^{-1}, \quad (12)$$

since the average time for a hop is inversely proportional to the transition probability. The energy relaxation rate r_E is then given by

$$\frac{\Delta E}{\Delta t} = -\frac{w_0 W}{p} \left[\frac{1-p}{p} + \exp\left(\frac{W}{k_B T}\right) \right]^{-1}. \quad (13)$$

At low enough temperatures, such that $k_B T < \frac{W}{\ln(\frac{1-p}{p})}$, and neglecting the temperature-dependence of w_0 , we obtain:

$$\frac{\Delta E}{\Delta t} \approx -\frac{w_0 W}{p} \exp\left(-\frac{W}{k_B T}\right)$$

To enable such behavior up to room temperature as observed in our experiment, p has to be larger than ~ 0.2 . If a uniform distribution of localized states over an energy interval is assumed, then for a localized state which lies in the middle of the energy band, the probability that all its neighboring sites are at higher energy is 0.25 when each site has two neighbors (chains) and 0.0625 in the case of four neighbors (planes), so our experiments suggest that carriers are localized in an one-dimensional (1D) structure.

For $\delta \approx 0.1$, the chains are the most obvious 1D feature in YBCO. However, apart of the chains there are also other possibilities of 1D structures, for example a cross-section of twin boundaries and the CuO_2 planes, in-plane stripes²⁹ or 1D charge density wave structures³⁰ which have all been reported in YBCO. However, the latter two are observed only at lower temperatures while the relaxation scenario which we are discussing is essentially the same at room temperature, apparently making these two possibilities less likely. In the insulator, with $\delta \approx 0.8$ there are no fully occupied chains and no twin boundaries, but the number of neighbors is small and there is some local chain formation³¹ in the basal plane, so the picture is also consistent with the proposed Fermi glass relaxation mechanism. The activation energies we obtain from the fits in Figures 4 and 5 are consistent with the values obtained in transient photoconductivity measurements⁵, and also with polaron binding energies obtained from fits to the mid-infrared conductivity spectra in YBCO²⁸. Although the value $E_a = 210$ meV obtained for the apical O vibration in the insulator is rather high, the implication of a deeper potential for carriers trapped in the Cu-O chains is consistent with calculations³³.

C. Discussion of the implications regarding the electronic structure

In our experiments the carriers are excited within 2.33 eV of the E_F . To determine the final states of the PE process one has to identify the relevant optical transitions at a given photon energy. Fortunately, for $\delta \approx 0.1$ YBCO, the optical transitions can be identified with help of LDA band structure calculations together with experimental ellipsometry data⁷. For c -axis polarized light the transitions are from the in- CuO_2 -plane $pd\sigma$ antibonding bands lying ~ 1 eV below the Fermi energy to the chain antibonding O(4)-Cu(1)-O(1) $pd\sigma$ band³². For light polarized parallel to the CuO_2 planes, transitions are largely (although not exclusively) with both initial and final states in the CuO_2 planes. The initial states lie ~ 2 eV below the Fermi energy, and the final states lie just above E_F . In addition, there are also some transitions between different Cu(1)-O(1) chain bands for light polarized along the b -axis.

In insulating YBCO with $\delta \approx 0.8$, optical transitions in this energy range are somewhat harder to identify, since due to strong electron correlation effects LDA calculations cannot be used as a reliable guide to the transitions involved.⁷ However, from the resonant Raman data on $\delta \approx 0.9$ samples Heyen *et al.*¹² conclude, that for light polarized parallel to the CuO_2 planes the transitions involved in the energy range up to ~ 2.5 eV are from the charge-transfer (CT) band to the upper Hubbard band (UHB). For c -axis polarized light, the transitions in the same energy range are assigned¹² to transitions from initial states in the occupied Cu(1) $d_{3z^2-r^2}$ -O(4) p_z dumbbell band to final states in the UHB which has also some Cu(2) $d_{3z^2-r^2}$ character.

Thus both in insulating and metallic YBCO, PE involves electronic transitions from planes to chains (or Cu(1)-O(4) dumbbells in the case of insulating YBCO) or vice versa for c -axis polarized light and mostly transitions in the CuO_2 planes for in-plane polarized light. However, since the PE carriers can partially relax before localization, the position of localized states relative to the E_F can not be inferred from the position of the initial PE states, which is only the upper boundary. Taking into account that in the present experiments only the PE carriers with energies above the phonon energy are detected, the observed localized states are at least one phonon energy away from the E_F . We cannot determine whether the localized states are above or below E_F since either holes or/and electrons can relax producing optical phonons.

In insulating YBCO with $\delta \approx 0.8$ the apical oxygen phonon shows significantly higher nonequilibrium phonon occupation numbers than the planar-buckling one. This is consistent with stronger localization in the basal plane

or in the Cu(1)-O(4) dumbbells. On the other hand, for $\delta \approx 0.1$, the difference between planar-buckling and apical-oxygen phonon nonequilibrium phonon effects is less dramatic, but somewhat surprising is the implication by the data that localized states exist also in the CuO₂ planes in the normal state of the optimally doped material.

The origin of the carrier localization is still not clear. Single-particle spectra from angle-resolved photoemission spectroscopy³⁵ imply the existence of a narrow band close to the Fermi energy. The origin of the band narrowing could be Holstein narrowing due to lattice polarons for example, or an effect of electronic correlations, or most likely both. The bandwidth observed experimentally is comparable to kT and lattice imperfections or defects can easily lead to carrier localization within such a band. However, it is also apparent from ARPES that a - possibly incoherent - background has non-zero spectral weight extending up to the Fermi energy, and these states could well be responsible for the temperature-dependent carrier relaxation. In any case, any tendency for carrier self-localization effects will be enhanced even further by the significant disorder present in these materials.

V. CONCLUSIONS

In conclusion, the pulsed resonant Raman scattering experiments show quite clearly - and independently of the model for the relaxation process - that some PE carrier relaxation proceeds via localized states. The comparison of the measurements with 1.5-ps and 70-ps laser pulses indicates that in metallic ($\delta \approx 0.1$) YBCO the effective room temperature PE-carrier lifetime before it reaches equilibrium is in the range of 10-100 ps, while for $\delta \approx 0.8$ the lifetime is shorter, probably in the 1 ps range. The present data and relaxation scenario are in agreement with recent photoinduced absorption measurements by Thomas *et al.*³⁴ who observed a long-lived relaxation component after laser photoexcitation in metallic YBa₂Cu₃O_{6.9} and Bi₂Sr₂CaCu₂O_{8+ δ} which they also attributed to carrier localization effects in the normal state of the superconductor.

Theoretically, relaxation via either polaronic states or a Fermi glass relaxation scenario can both reproduce the experimental temperature dependence of the carrier relaxation, the latter model suggesting that the states through which the relaxation takes place are in one-dimensional chains. Although the position of the localized states in real space can be discussed with some degree of certainty, we can only state that the localized states lie within a 2.3 eV wide band around E_F and relaxation measurements - either Raman or time-resolved photoinduced absorption - with different laser wavelengths would be necessary to determine their energy more precisely. The presence of localized states in the optimally doped superconductors is believed to have important consequences both for superconductivity and hot-carrier device design using these materials.

-
- ¹ See for example reviews by Z.X.Shen et al, *Science* **267**, 343 (1995) or A.S.Alexandrov and N.F.Mott, *Rep.Prog.Phys.* **57**, 1197 (1995), N.F. Mott, *Physica C* **205**, 191 (1993).
- ² J.Ranninger and S.Robaszkiewicz, *Physica B* **135**, 468 (1985), J.Ranninger, *Z.Phys.B.* **84**, 167 (1991).
- ³ D.Mihailovic *et al.*, *Phys. Rev.* **B45**, 8016 (1992); T.Egami and S.J.L.Billinge, *Prog. Mat. Sci.* **38**, 359 (1994).
- ⁴ M.J.Holcomb, J.P. Collman and W.A.Little, *Phys.Rev.Lett.* **73**, 2306 (1994)
- ⁵ G.Yu *et al.* *Phys. Rev Lett.* **67**, 2581, (1991); *ibid*, *Phys. Rev. B* **45**, 4964 (1992).
- ⁶ I.Poberaj and D.Mihailovic, *Phys. Rev.* **B50**, 6426 (1994).
- ⁷ J. Kircher, M.K. Kelly, S. Rashkeev, A. Alouani, F. Fuchs, M. Cardona, *Phys. Rev.* **B44**, 217 (1991).
- ⁸ R. Loudon, *Proc. of the Royal Soc.* **A 275**, 218 (1963).
- ⁹ See for example: M. Cardona, p. 40, *Light Scattering In Solids II*, editors: M. Cardona and G. Güntherodt, (Springer-Verlag, Berlin 1983).
- ¹⁰ T. Gong, L.X. Zheng, W. Xiong, W. Kula, Y. Kostoulas, R. Sobolewski, P.M. Fauchet, *Phys. Rev.* **B47**, 14495 (1993).
- ¹¹ E.T. Heyen, S. N. Rashkeev, I.I. Mazin, O.K. Andersen, R. Liu, M. Cardona, O. Jepsen, *Phys. Rev. Lett.* **65**, 3048 (1990).
- ¹² E.T. Heyen, J. Kircher, M. Cardona, *Phys. Rev.* **B45**, 3037 (1992).
- ¹³ R.D. Larrabee, *J. Opt. Soc. Am.* **49**, 619 (1959).
- ¹⁴ A. Bock, *Phys. Rev.* **B51**, 15506 (1995).
- ¹⁵ J.H.Bechtel, *J. Appl. Phys.* **46**, 1585 (1975).
- ¹⁶ T. Mertelj, PhD. Thesis, December 1995.
- ¹⁷ A. Junod, Specific Heat of High Temperature Superconductors: a Review, *Physical Properties of High Temperature Superconductors II*, (World Scientific, New York 1990).
- ¹⁸ M.J. Holcomb, C.L. Perry, J.P. Collman, W.A. Little, submitted to *Phys. Rev. B*.

- ¹⁹ I. Fugol, V. Samovarov, A. Ratner, V. Zhuravlev, G. Saemann-Ichenko, M. Lippert, B. Holzapfel, *Physica C* **216**, 391 (1993).
- ²⁰ B. Friedel, C. Thomsen, H.-U. Habermeier, M. Cardona, *Sol. Stat. Comm.* **78**, 291 (1991).
- ²¹ D. Mihailovic, K.F. McCarthy, D.S. Ginley, *Phys. Rev.* **B47**, 8910 (1993).
- ²² B. Friedel, C. Thomsen, M. Cardona, *Phys. Rev. Lett.* **65**, 915 (1990).
- ²³ D. Mihailovic, K.F. McCarthy, D. S. Ginley, *Ferroelectrics* **130**, 107 (1992).
- ²⁴ K. Seeger, *Semiconductor Physics*, section 6.11-6.12 (Springer Series in Solid State Sciences, Berlin Heidelberg, 1985).
- ²⁵ N.F. Mott, E.A. Davis, *Electronic Processes in Non-Crystalline Materials*, (Clarendon Press, Oxford 1979).
- ²⁶ A.R. Long, *Advances in Physics* **31**, 553 (1982).
- ²⁷ S.R. Elliott, *Advances in Physics* **36**, 135 (1987).
- ²⁸ D.Mihailovic et al, *Phys.Rev.B*, **42**, 7989-7997 (1990).
- ²⁹ M. Missori, A. Bianconi, H. Onyanagi, H. Y. Yamaguchi, *Physica C* **235-240**, 1245 (1994).
- ³⁰ H.L. Edwards, D.J. Derro, A.L. Barr, J.T. Markert, A.L. de Lozanne, *Phys. Rev. Lett.* **75**, 1387 (1995).
- ³¹ N.H. Andersen, B. Lebech, H.F. Poulsen, *Physica C* **172**, 31 (1990).
- ³² S. Gopalan, J. Kircher, O.K. Andersen, O. Jepsen, M. Auliani, M. Cardona, *Physica C* **185-189**, 1474 (1991).
- ³³ J.Ranninger and J.M.Robin, *Phys. Rev.Lett.***74**, 4027 (1995)
- ³⁴ T.N. Thomas, C.J. Stevens, S. Choudary, J.F. Ryan, D. Mihailovic, T. Mertelj, L. Forro, G. Wagner, J.E. Evetts, *Phys. Rev.* **B** 53, 12436 (1996).
- ³⁵ B.O.Wells et al, *Phys.Rev.Lett* **74**, 964 (1995),

FIG. 1. The phonon Raman spectra of the apical-oxygen phonon (a) and the planar buckling phonon (b) in $\delta \approx 0.1$ YBCO as a function of temperature at the 70-ps excitation. The spectra are vertically shifted for clarity. At lower temperatures the planar-buckling-phonon lineshape is distorted due to the low spectrometer resolution.

FIG. 2. The nonequilibrium phonon heating as a function of temperature for the apical-oxygen phonon (a) and the planar buckling phonon (b) in the $\delta \approx 0.8$ YBCO. Error bars represent standard errors obtained from fits of the Raman intensities.

FIG. 3. The nonequilibrium phonon heating as a function of temperature for the apical-oxygen phonon (a) and the planar buckling phonon (b) in the $\delta \approx 0.1$ YBCO. Error bars represent errors obtained from fits of the Raman intensities.

FIG. 4. Arrhenius plots of $n_{neq}^{\delta=0.8}$ versus temperature for the apical-oxygen phonon (a), and the planar buckling phonon (b) in the $\delta \approx 0.8$ YBCO. The solid lines are Arrhenius fits to the data. Error bars represent errors obtained from fits of S and A intensities.

FIG. 5. Arrhenius plots of $n_{neq}^{\delta=0.1}$ versus temperature for the apical-oxygen phonon (a) and the planar buckling phonon (b) in the $\delta \approx 0.1$ YBCO. The solid lines are Arrhenius fits to the data. Error bars represent errors obtained from fits of S and A intensities.

FIG. 6. The calculated nonequilibrium phonon occupation number (4) as a function of the inverse PE-carrier relaxation time, τ_c^{-1} , for two different pulse lengths and different phonon lifetimes, τ_p . The number of photons per pulse as well as ratio c_{pc}/N_p are the same for both pulse lengths. In this model τ_c^{-1} is proportional to the PE-carrier energy relaxation rate r_E .

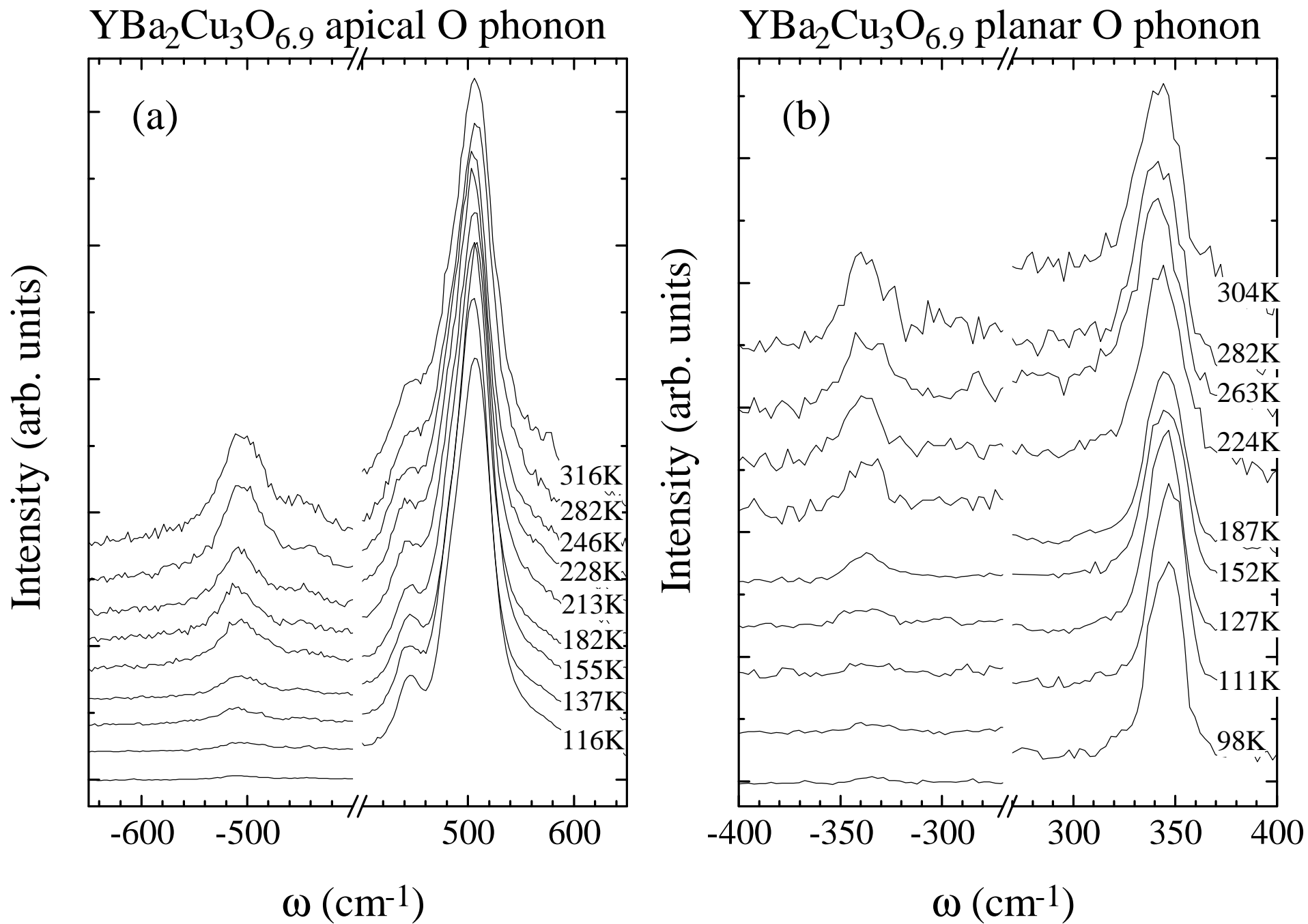


Fig.1

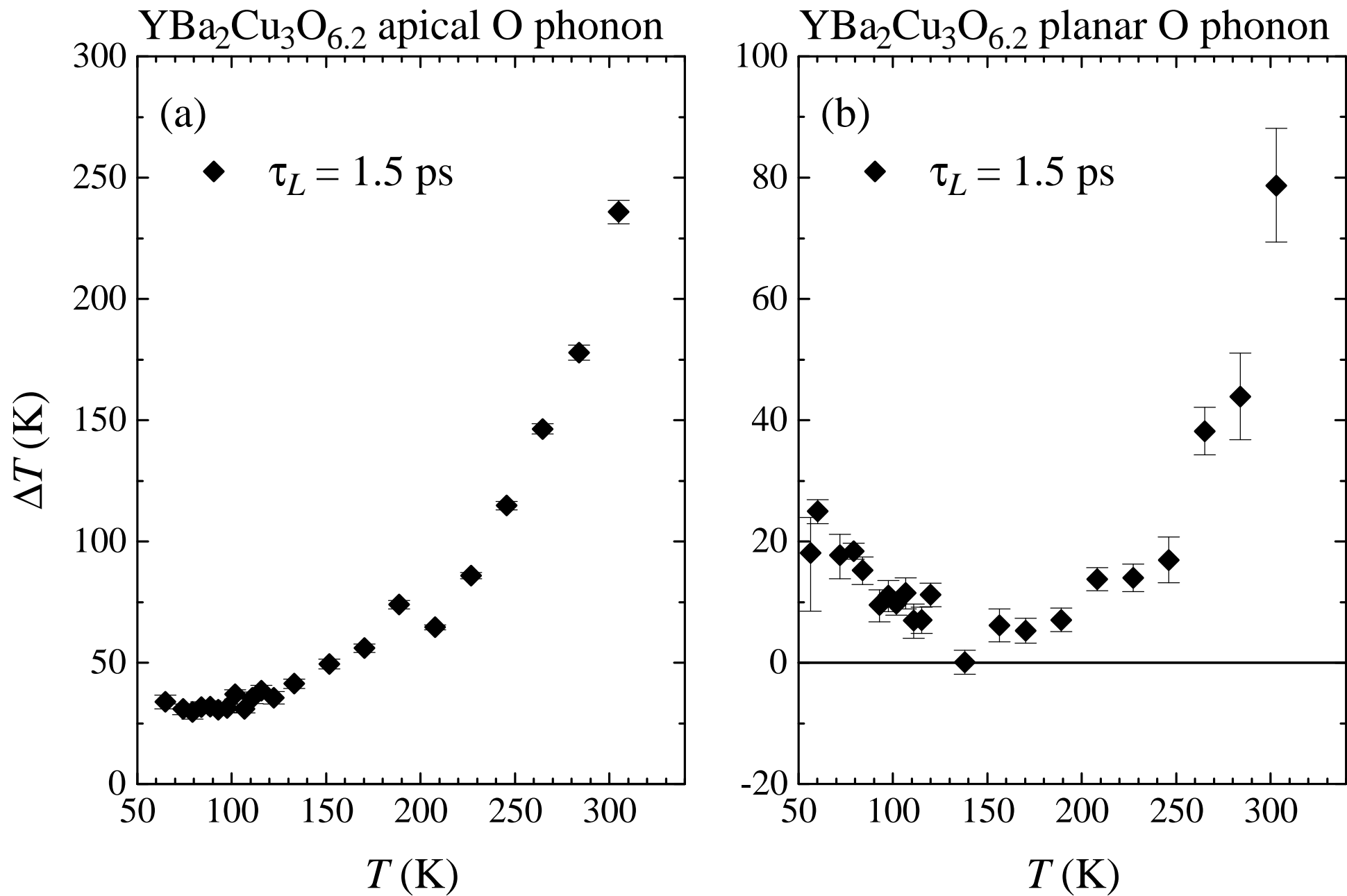


Fig.2

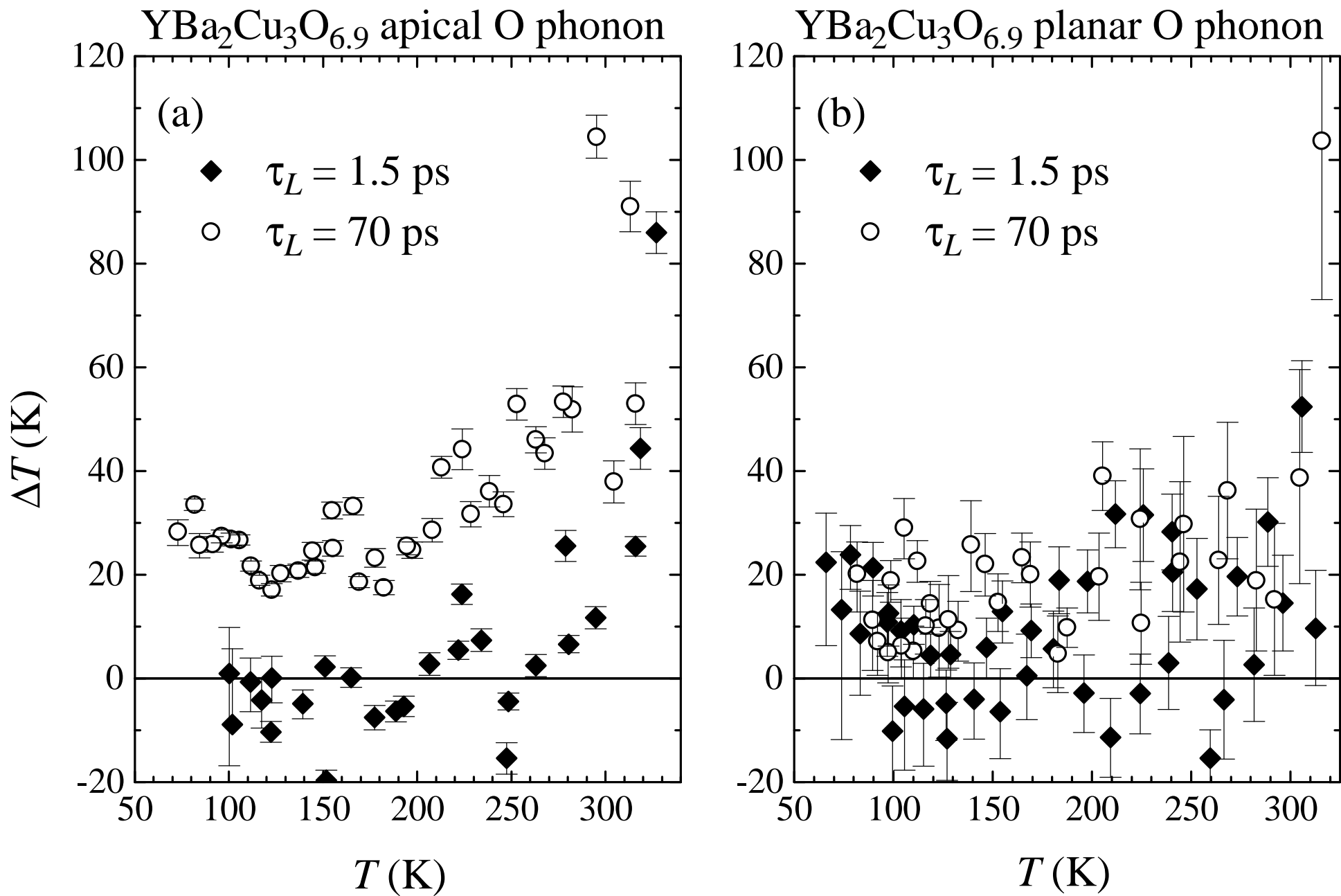


Fig.3

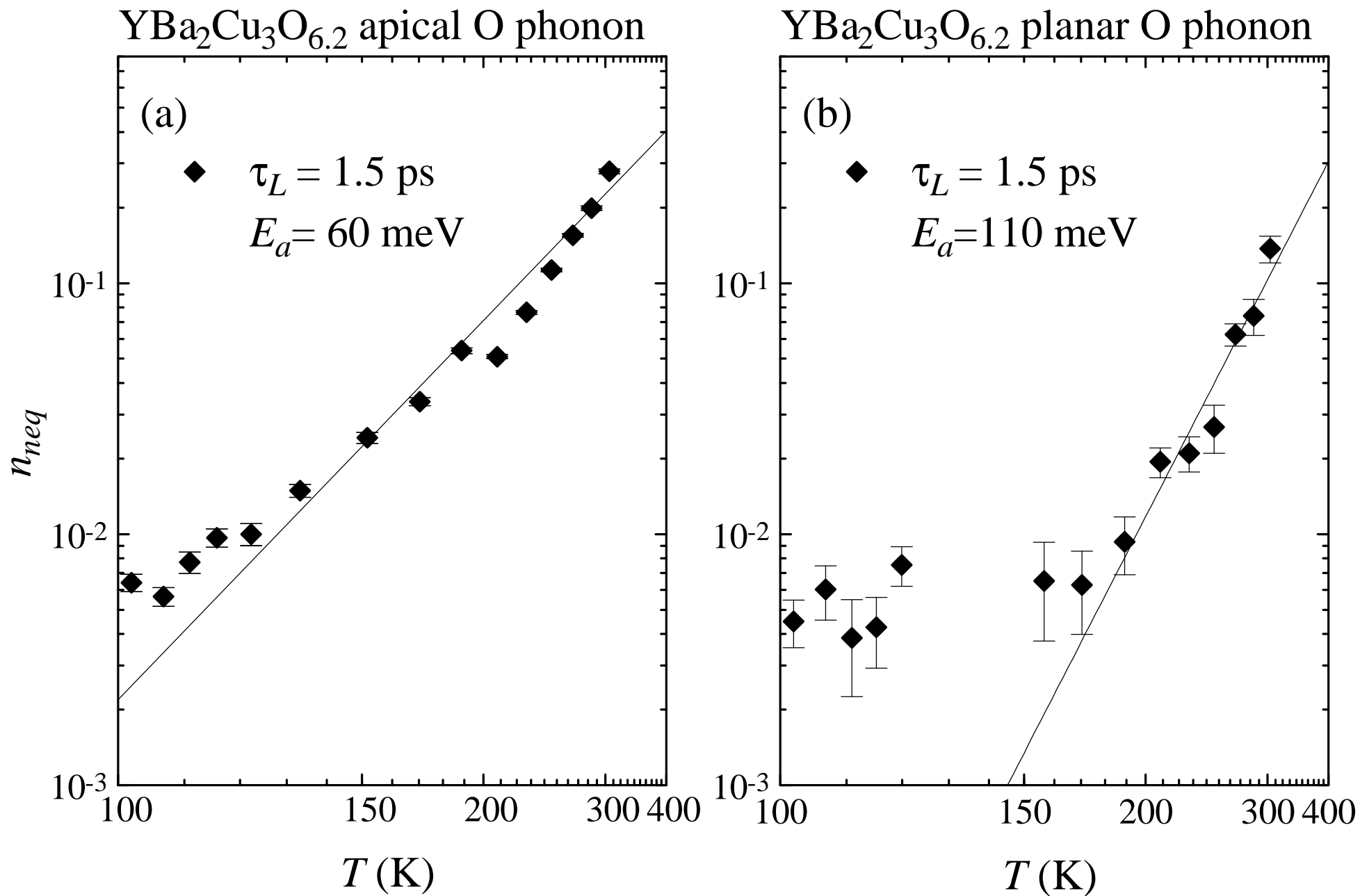


Fig. 4

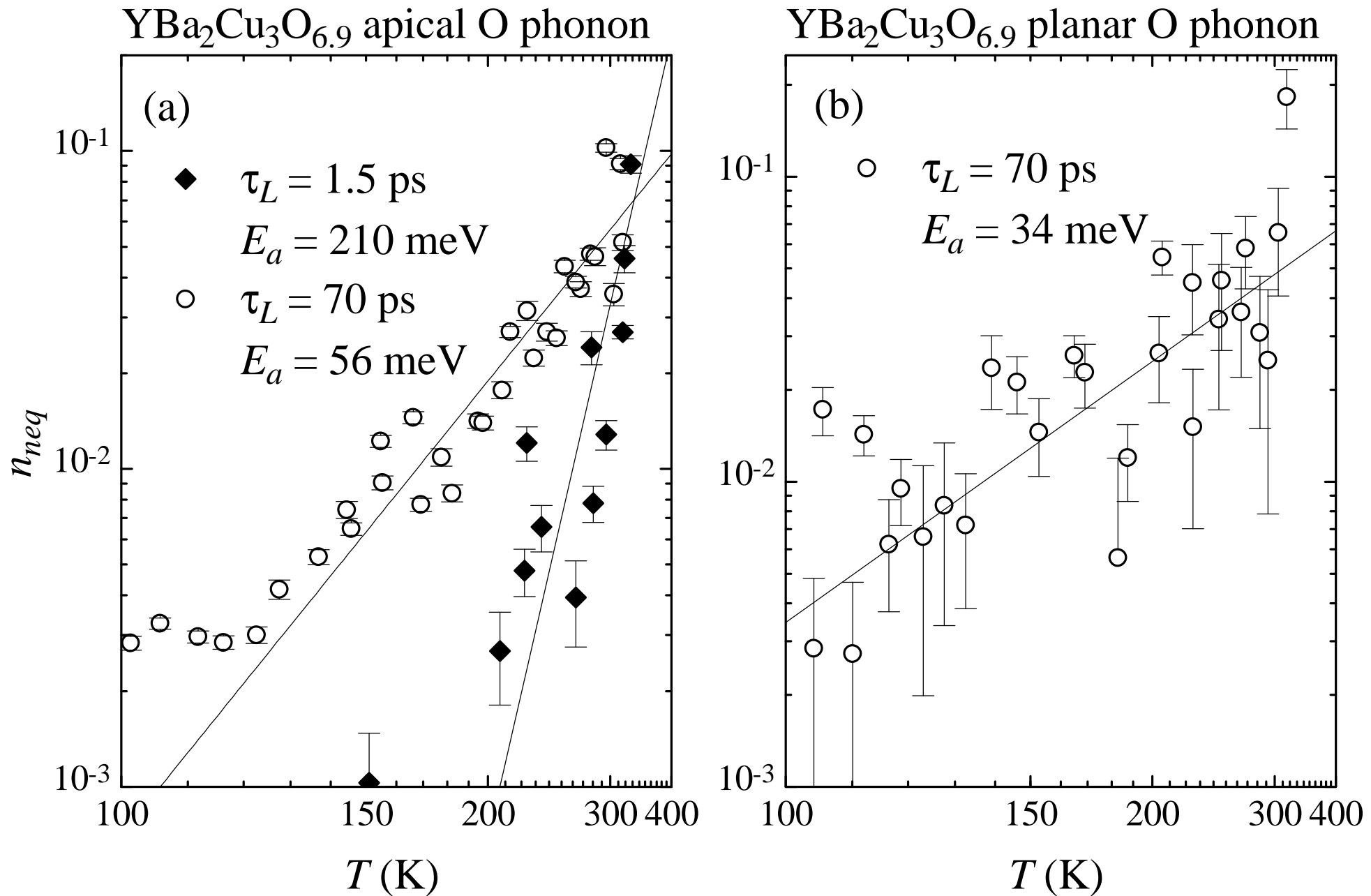


Fig. 5

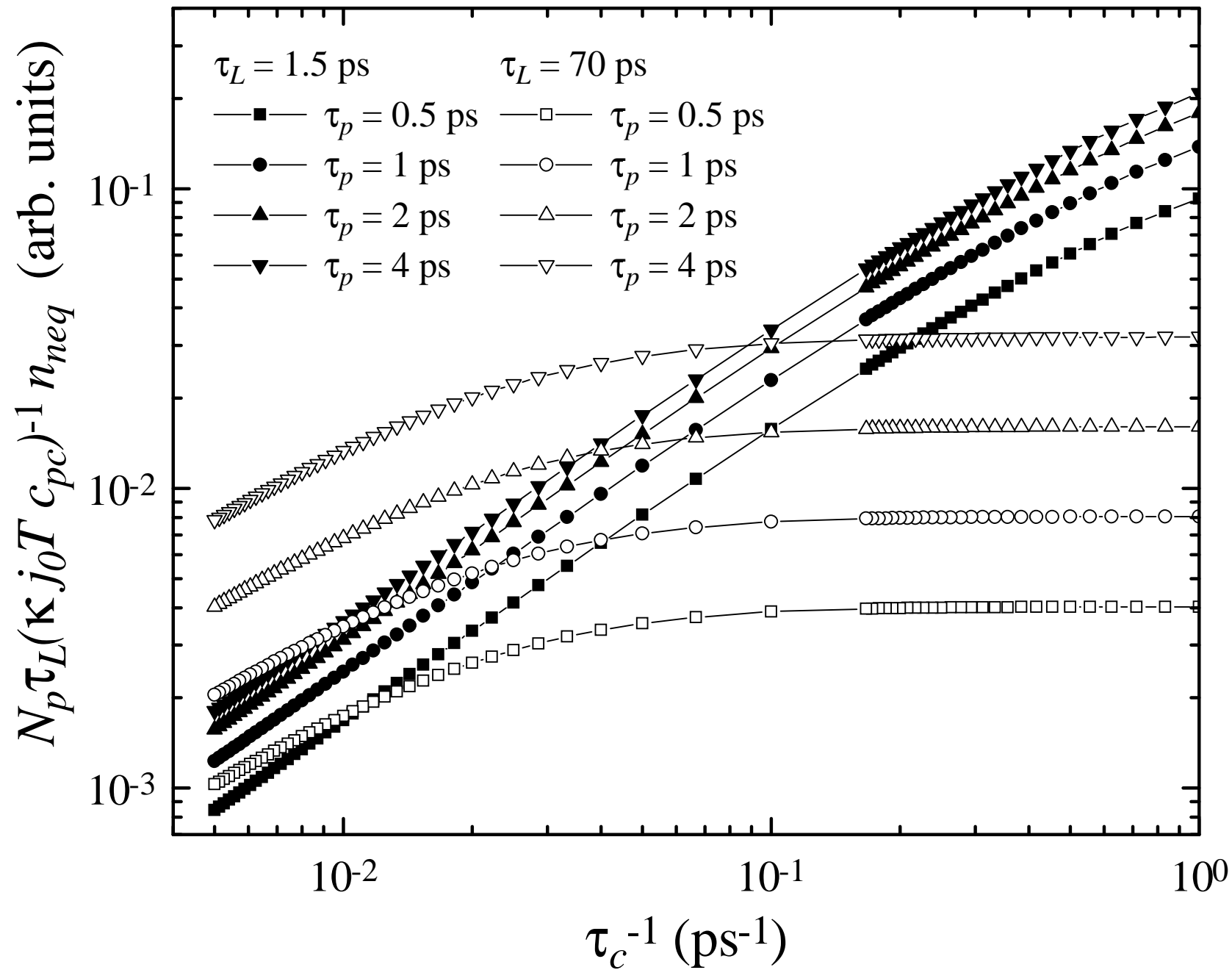


Fig. 6